Temperature-dependent magnetoconductance in quantum wires: Effect of phonon scattering

S. K. Lyo
Sandia National Laboratories, Albuquerque, New Mexico 87185, USA

Danhong Huang
Air Force Research Laboratory (AFRL/VSSS), Kirtland Air Force Base, New Mexico 87117, USA

(Received 23 April 2003; published 26 September 2003)

A rigorous numerical formalism is presented for the conductance in quasi-one-dimensional systems dominated by phonon and elastic scattering. The formalism is applied to study the effects of phonon scattering and the interface-roughness scattering at low temperatures (T) on the T-dependent electron conductance in a multilevel single quantum wires (SQWR's) and tunnel-coupled double quantum wires (DQWR's) under a perpendicular magnetic field B. The effect of phonon scattering is significant when the thermal energy k_BT is comparable to the energy separation between the Fermi level and the nearest unoccupied sublevel in SQWR's and to the tunneling gap energy in DQWR's. While the magnetoconductance decreases with increasing T in general, it displays a strikingly opposite behavior in certain regimes of B and T in DQWR's because of the field-induced separation of the initial and final scattering-state wave functions into the two separate quantum wires.

DOI: 10.1103/PhysRevB.68.115317 PACS number(s): 72.20.My, 73.40.Gk, 72.20.Fr, 73.40.Kp

I. INTRODUCTION

Transport properties of low-dimensional structures are of current interest for many novel physical phenomena and possible applications for new devices. A number of recent studies have focused on the low-temperature conduction in quantum wires.[1–10] Most of the past investigations deal with low-temperature elastic-scattering effects[1–8] and magnetic-field effects[5,6,8,9] in single-quantum-well wires (SQWR's). The effect of tunneling between two quantum wires in tunnel-coupled double-quantum-well wires (DQWR's) was studied recently.[8] In these systems, scattering by impurities, interface roughness, and phonons plays a dominant role for the momentum relaxation. In this paper, we assess the relative importance of elastic- and inelastic-scattering mechanisms as a function of the temperature T and the magnetic field. In multisublevel quantum wires, intersublevel electron-phonon scattering is very important in momentum-relaxation processes as will be shown later. In this case, the standard quasi-elastic-scattering approximation does not yield an accurate result for electron-phonon scattering because the phonon energy can be comparable to the electron energy. Therefore, a rigorous method for treating combined elastic and phonon scattering is necessary. We develop a formalism which yields the conductance to a desired accuracy for a general quasi-one-dimensional electronic structure and apply the result to study the temperature-dependent conductance of SQWR's and tunnel-coupled DQWR's illustrated in Fig. 1. We study high-quality wires where the localization length is larger than the sample length. We neglect the Luttinger liquid effect.

We examine the effect of phonon and interface-roughness scattering in the presence of a perpendicular magnetic field B. Scattering by ionized impurities can be treated within the same formalism as that of interface-roughness scattering but will be neglected assuming that the dopants are far away from the quantum well (QW) for high-quality modulation-doped samples. We find that the effect of phonon scattering can be important even at low temperatures (e.g., $T=2-4$ K). In SQWR's, the zero-temperature conductance is sharply enhanced for elastic scattering following the depopulation of a sublevel at low temperatures.[6,8] This enhancement becomes severely suppressed even at these low temperatures due to phonon scattering. Although the magnetoconductance is expected to decrease with increasing temperature in general, we find that the conductance can rise sharply as a function of T in DQWR's in certain regimes of B and T because of the effect arising from the field-induced spatial separation of the initial- and final-state wave functions involved in backscattering into separate quantum wells (QW's). Phonon scattering suppresses the conductance eventually at high temperatures in this case, yielding a peak in the T dependence of the conductance.

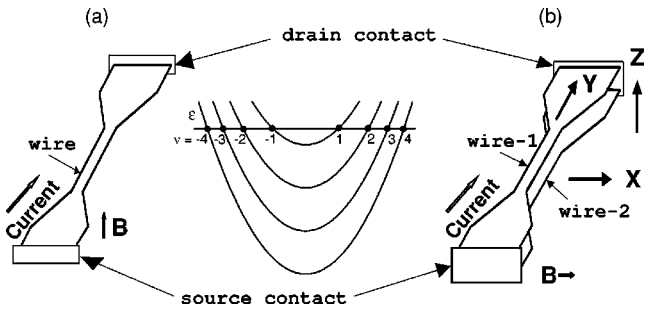

FIG. 1. (a) A schematic diagram of a SQWR. A narrow channel is formed by applying a negative bias on the top split metallic gate, not shown. (b) A schematic diagram for DQWR. Electrons tunnel between the wires through the $Al_xGa_{1-x}As$ barrier in the z direction. The current flows along the y direction. A magnetic field B lies in the x direction for the double wires and in the z direction for the single wire. The curves in the inset illustrate the 1D energy dispersion.

II. MULTISUBLEVEL MAGNETOTRANSPORT

We consider transport for a general quasi-one-dimensional electronic structure characterized by the energy dispersion ε_j with $j=\{n,k\}$. Here, n denotes the sublevel index $n=0,1,\ldots$ and k is the wave number along the wire in the absence of scattering but in the presence of magnetic field B. The dispersion curves ε_j do not cross. The meaning of the sublevel index n will be specified later in Sec. IV, where application is made to SQWR's and DQWR's. We expand the nonequilibrium distribution f_j as $f_j=f_0(\varepsilon_j)+g_j[-f_0'(\varepsilon_j)]eE$, where the second term represents the linear deviation from the equilibrium Fermi function $f_0(\varepsilon_j)$ caused by an external dc electric field E. Here $f_0'(\varepsilon_j)$ is the first derivative of the Fermi function with respect to the energy. The Boltzmann equation for the magnetotransport of the electrons along the wire (y) direction in the presence of both inelastic (phonon) and elastic (impurity or interface roughness) scattering is then given by[11,12]

$$v_j+\frac{2\pi}{\hbar}\sum_{j'}|I_{j',j}|^2(g_{j'}-g_j)\,\delta(\varepsilon_j-\varepsilon_{j'})+P_j=0, \quad (1)$$

where $v_j=\hbar^{-1}d\varepsilon_j/dk$ is the group velocity of the electrons. In Eq. (1), $I_{j',j}$ is the scattering matrix from impurities or interface roughness. The case for elastic scattering with $P_j=0$ was studied earlier by the authors.[8] The quantity P_j represents the contribution from the electron-phonon interaction and is given by[12]

$$P_j=\frac{2\pi}{\hbar}\sum_{j',s,\mathbf{q},\pm}|V_{j'j}^{s\mathbf{q}}|^2(f_{j'}^{(\mp)}+n_{s\mathbf{q}})(g_{j'}-g_j)\times\delta(\varepsilon_j-\varepsilon_{j'}\pm\hbar\omega_{s\mathbf{q}})\,\delta_{k',k\pm q_y}, \quad (2)$$

where $V_{j'j}^{s\mathbf{q}}$ is the screened electron-phonon interaction[10] defined by $\langle n'k'|V_{s,\mathbf{q}}^{\text{e-ph}}|nk\rangle=V_{j'j}^{s\mathbf{q}}\delta_{k',k+q_y}$ and the upper (lower) sign corresponds to the one-phonon emission (absorption) process. Deformation-potential and piezoelectric interactions are considered. In Eq. (2), $f_{j'}^{(-)}=f_0(\varepsilon_{j'})$, $f_{j'}^{(+)}=1-f_{j'}^{(-)}$, and $n_{s\mathbf{q}}$ is the Boson function for the phonon of mode s with energy $\hbar\omega_{s\mathbf{q}}$ and wave vector $\mathbf{q}$.

The conductance of the system is given in terms of g_j in Eq. (1) (Ref. 8),

$$G(B)=\frac{2e^2}{hL_y}\int_0^{+\infty}d\varepsilon[-f_0'(\varepsilon)]S^{\dagger}\tilde{g}, \quad (3)$$

where L_y is the length of the wire and $S^{\dagger}$ is the transpose of a column matrix S with elements $s_\nu=v_\nu/|v_\nu|$, which is the sign of the slope of the dispersion curve at point ν. The points $\nu=1,2,\ldots$ represent the discrete horizontal points $(k_\nu,\varepsilon_{k_\nu})$ on the energy-dispersion curves with a common energy $\varepsilon=\varepsilon_j=\varepsilon_{k_\nu}$. At zero temperature $T=0$, these points in Eq. (3) are the Fermi points. Avoiding the case where any of these points is an energy extremum, we number these points as

$$\nu=-N,-N+1,\ldots,-1,1,\ldots,N-1,N \quad (4)$$

as illustrated in Fig. 1 for $N=4$ in the inset. In Eq. (3), $\tilde{g}$ is a column matrix with elements $\tilde{g}_\nu=g_\nu-g_N$.[8] The replacement $\tilde{g}\to g$ in Eq. (3) does not make any difference because $\Sigma_\nu s_\nu=0$. Therefore, the dimensions of S and $\tilde{g}$ are restricted to $2N-1$ in Eq. (3), discarding the last point $\nu=N$ with $\tilde{g}_N=0$. The real necessity for eliminating one of the $2N$ points arises from the absence of the inverse of the full $2N\times 2N$ scattering matrix (U to be defined below) between the $2N$ points in solving the Boltzmann equation as shown earlier.[8]

In this paper, we study symmetric dispersion curves for simplicity and use $g_{-\nu}=-g_\nu$ to obtain

$$g_\nu=\tilde{g}_\nu-\frac{1}{2}\tilde{g}_{-N}, \quad \tilde{g}_N\equiv 0. \quad (5)$$

This assumption is relevant to all SQWR's and symmetric DQWR's in magnetic fields. The set of the wave number k_ν depends on the energy ε. Hereafter, we put this ε dependence specifically on all quantities, e.g., $g_\nu\equiv g_\nu(\varepsilon)$. Dividing each term in Eq. (1) by $|v_j|$, converting $\Sigma_{k'}\propto\int d\varepsilon/|v_{j'}|$, and using the above definitions we find

$$U(\varepsilon)\tilde{g}(\varepsilon)+v^{-1}(\varepsilon)P(\varepsilon)=-S(\varepsilon) \quad (6)$$

or

$$\tilde{g}(\varepsilon)=-U^{-1}(\varepsilon)[S(\varepsilon)+v^{-1}(\varepsilon)P(\varepsilon)]. \quad (7)$$

Here, $\tilde{g},S,P$ are column matrices of the order of $2N-1$ excluding the end point $\nu=N$ for each energy ε, v is a diagonal matrix of the same order with the elements $v_{\nu,\nu'}=\delta_{\nu,\nu'}|v_\nu|$, and U is the $(2N-1)\times(2N-1)$ square elastic-scattering matrix given by[8]

$$U_{\nu,\nu'}=U_{\nu',\nu}=\frac{L_y}{\hbar^2}\frac{|I_{\nu'\nu}|^2}{|v_{\nu'}v_\nu|} \quad \text{for} \quad \nu\neq\nu' \quad (8)$$

and

$$U_{\nu,\nu}=-\sum_{\nu'\neq\nu}U_{\nu,\nu'}. \quad (9)$$

In Eqs. (8) and (9), ν and ν' exclude the end point as discussed above. Otherwise, the quantity U^{-1} becomes singular for the full $2N\times 2N$ matrix.[8]

In order to carry out the $\mathbf{q}$ summation in Eq. (2), we introduce a cylindrical coordinate $q_x=q_\perp\cos\phi$, $q_z=q_\perp\sin\phi$, $q=\sqrt{q_\perp^2+q_y^2}$, and a transform

$$\sum_{\mathbf{q}}\delta_{q_y,k'-k}=\frac{L_xL_z}{(2\pi)^2}\int q_\perp dq_\perp\int d\phi\,\delta_{q_y,k'-k}=\frac{L_xL_z}{(2\pi)^2}\int qdq\int d\phi\,\delta_{q_y,k'-k}.$$

We now introduce the Debye approximation at low temperatures and assume $\hbar\omega_{s\mathbf{q}}=\hbar c_s q$, where c_s is the sound velocity for the phonon mode s. Carrying out the q integration

through the energy δ function and converting the k' summation into the ε' integration in Eq. (2), we find

$$\frac{P_\nu(\varepsilon)}{|v_\nu(\varepsilon)|}=\frac{\Omega}{(2\pi)^2\hbar^2}\sum_{n',s,\pm}\int d\varepsilon'\frac{q}{\hbar c_s}\theta[\pm(\varepsilon'-\varepsilon)]\times\int d\phi\frac{|V^{s\mathbf{q}}_{j'\nu}(\varepsilon,\varepsilon')|^2}{|v_{j'}(\varepsilon')v_\nu(\varepsilon)|}\times(f^{(\mp)}_{j'}+n_{s\mathbf{q}})[g_{j'}(\varepsilon')-g_\nu(\varepsilon)], \tag{10}$$

where $\theta(\varepsilon)$ is the unit step function, $\Omega=L_xL_yL_z$ is the sample volume, and

$$\hbar c_s q=|\varepsilon-\varepsilon'|,\quad |q_y|=|k'-k|,\quad \text{and}\quad q_\perp=\sqrt{q^2-q_y^2}. \tag{11}$$

The ε' integration excludes the region where $q_\perp$ becomes imaginary.

III. MATRIX EQUATION APPROACH

Noting that P in Eq. (7) contains $\tilde{g}$, the latter can be found using an iteration method. However, we present here a more rigorous method for the solution of the Boltzmann Equation (6) that allows us to control the accuracy to a desired degree. For this purpose, let us define for the scattering-out term on the right-hand side of Eq. (10),

$$W^{(o)}_\nu(\varepsilon)=\frac{\Omega}{(2\pi)^2\hbar^2}\sum_{n',s,\pm}\int d\varepsilon'\frac{q\,\theta[\pm(\varepsilon'-\varepsilon)]}{\hbar c_s}\times\int d\phi\frac{|V^{s\mathbf{q}}_{j'\nu}(\varepsilon,\varepsilon')|^2}{|v_\nu(\varepsilon)v_{j'}(\varepsilon')|}(f^{(\mp)}_{j'}+n_{s\mathbf{q}}), \tag{12}$$

with the condition given in Eq. (11). We now replace the ε' integration in the scattering-in term in Eq. (10) with a summation over the energy points uniformly spaced by a sufficiently small energy interval $\delta\varepsilon$. We further introduce a new index $t=\{\ell,m\}$, where ℓ counts the k points from the left to the right "horizontally" for a given energy and m indicates the energy in the above "vertical" ε' subdivision. Defining

$$W_{t,t'}=\frac{\Omega\,\delta\varepsilon}{(2\pi)^2\hbar^2}\sum_{s,\pm}\frac{q}{\hbar c_s}\theta[\pm(\varepsilon'-\varepsilon)]\times\int d\phi\frac{|V^{s\mathbf{q}}_{t',t}|^2}{|v_t v_{t'}|}(f^{(\mp)}_{t'}+n_{s\mathbf{q}}), \tag{13}$$

we can recast Eq. (10) into a matrix equation

$$\frac{P_t}{|v_t|}+W^{(o)}_t g_t=\sum_{t'}W_{t,t'}g_{t'}. \tag{14}$$

This equation can be rewritten, by converting g into $\tilde{g}$ according to Eq. (5), as

$$\frac{P_t}{|v_t|}=\sum_{t'}\tilde{W}_{t,t'}\tilde{g}_{t'}, \tag{15}$$

where

$$\tilde{W}_{t,t'}=(W_{t,t'}-\delta_{t,t'}W^{(o)}_t)(1-\tfrac{1}{2}\delta_{\ell',-N_{m'}}) \tag{16}$$

and $t=\{\ell,m\}$ and $t'=\{\ell',m'\}$. It is understood that the indices t,t' exclude the rightmost point for each of the energy indices m,m'. In Eq. (16), $\ell'=-N_{m'}$ signifies the leftmost point for the energy index m' according to the notation introduced in Eq. (4). Inserting Eq. (15) into Eq. (6), we get the matrix equation

$$[U+\tilde{W}]\tilde{g}=-S \tag{17}$$

and its solution

$$\tilde{g}=-[U+\tilde{W}]^{-1}S. \tag{18}$$

We note that the matrix U for the elastic scattering is block diagonal with respect to the energy index m, namely, $U_{t,t'}\propto\delta_{m,m'}$. The phonon-scattering matrix $\tilde{W}$ introduces the coupling between a pair of blocks. In this notation, S and $\tilde{g}$ are column matrices, where the mth set of array consists of $2N_m-1$ points belonging to the same energy index m and representing the wave numbers $k_{\ell m}$. In this notation, the conductance given in Eq. (3) can be rewritten as

$$G(B)=\left(\frac{2e^2}{hL_y}\right)\delta\varepsilon\sum_t[-f_0'(\varepsilon_t)]S_t\tilde{g}_t. \tag{19}$$

IV. NUMERICAL RESULTS AND DISCUSSIONS

In our numerical calculations, we study a GaAs wire sandwiched by $Al_{0.3}Ga_{0.7}As$ barriers and assume the following parameters: electron effective mass $m_B=0.073m_0$ in the barrier with free-electron mass m_0, $m^*=0.067m_0$ in the well, bulk dielectric constant $\kappa=12$, longitudinal sound velocity $c_\ell=5.14\times10^5$ cm/sec, transverse sound velocity $c_t=3.04\times10^5$ cm/sec, GaAs mass density $\rho=5.3$ g/cm^3, piezoelectric constant $h_{14}=1.2\times10^7$ V/cm, deformation-potential coefficient $D=-9.3$ eV, and level broadening $\gamma_j=0.16$ meV.[10] The broadening is employed at the bottom of the sublevels where the one-dimensional density of states diverges. The Debye approximation is employed for the acoustic phonons at low temperatures.

We also assume that elastic scattering is dominated by the interface roughness of a monolayer fluctuation $\delta b=5$ Å with a Gaussian correlation length given by $\Lambda_x=\Lambda_y=30$ Å.[8] The interface roughness is assumed to exist only at one (two) interface(s) between GaAs QW and the $Al_{0.3}Ga_{0.7}As$ barrier in the growth sequence in the z direction for single (double) QW's as is well known. We assume a conduction-band offset of 270 meV in the z direction. For SQWR's (samples 1 and 2), the sublevels are due to a parabolic confinement in the x direction with a uniform level separations of $\hbar\omega_x$ at $B=0$, while the electrons are in the ground sublevel in the z direction in a rectangular well. For

TABLE I. SQWR's with the QW width L_z, the ground-second level separation $\Delta\mathcal{E}_z$, one-dimensional electron density n_{1D}, the uniform channel sublevel separation $\hbar\omega_x$, the wire length L_y, and the chemical potential μ (at $T=0$ K and $B=0$) relative to the bottom of the ground level.

Sample no.	L_z (Å)	$\Delta\mathcal{E}_z$ (meV)	n_{1D} (10^6 cm^{-1})	$\hbar\omega_x$ (meV)	L_y (μm)	μ (meV)
1	210	29	1	2.5	10	4.81
2	210	29	1	1.6	10	3.46

DQWR's (samples 3 and 4), the sublevels are due to the tunnel-split doublet in the z direction in a rectangular potential, while the electrons are in the ground sublevel in the x direction in a parabolic potential. The parameters for samples 1 and 2 are given in Table I and the parameters for samples 3 and 4 are given in Table II. Here, $\hbar\omega_x=1$ meV corresponds to the size of the wave function $\sim 2\ell_x = 2\sqrt{\hbar c/m^*\omega_x}=477$ Å in the x direction for $m^*=0.067m_0$. Other parameters will be given in the corresponding figure captions.

For SQWR's, the magnetoconductance depends sensitively on B in the z direction. In this case, B modifies the eigenvalues in the perpendicular direction according to

$$\varepsilon_{nk}=\left(n+\frac{1}{2}\right)\hbar\Omega_x+\frac{\hbar^2k^2}{2m^{**}}, \tag{20}$$

where $n=0,1,\ldots,$ $\Omega_x=\sqrt{\omega_c^2+\omega_x^2}$, $\omega_c=eB/m^*c$, and $m^{**}=m^*/[1-(\omega_c/\Omega_x)^2]$.[5,8] The ground level wave function in the z direction is not affected by B and is calculated numerically. In the x direction, however, the argument of the harmonic wave functions is modified as $(x+\Delta x_k)/\ell_{cx}$, where $\ell_{cx}=\sqrt{\hbar c/m^*\Omega_x}$ and the B-induced shift equals $\Delta x_k = k\hbar\omega_c/m^*\Omega_x^2$. The expressions for the matrix elements for the interface roughness interaction $U_{\nu,\nu'}$ are worked out in terms of these wave functions in Ref. 8.

For DQWR's, interesting properties of the magnetoconductance occur when B lies in the x direction. In this case, the energy-dispersion parabola in QW2 is displaced by $\Delta k = d/\ell_c^2$ in k space (in the y direction) relative to that in QW1, where d is the well-to-well distance and $\ell_c=\sqrt{\hbar c/eB}$ is the magnetic length. An anticrossing gap opens at the intersecting point of these two parabolas due to tunneling, separating the upper and lower branches.[13] The gap passes through the chemical potential with increasing B. For symmetric double QWs, for example, the z-wave functions are symmetric (antisymmetric) at the lower (upper) gap edge (i.e., at the symmetry axis $k=0$). For k states inside the gap, the z-wave functions with $k>0$ are localized mostly in one of the QW's while those with $k<0$ are localized mostly in the other QW.[13,14] The wave functions and eigenvalues are calculated numerically.[8] In the x direction, we assume a narrow rectangular well with only the ground level occupied. This wave function is not affected by B. The matrix elements for $U_{\nu,\nu'}$ are calculated in terms of these wave functions as in our earlier work.[8]

For electron-phonon scattering, we use screened deformation-potential and piezoelectric interactions. Detailed expressions for $V^{s\mathbf{q}}_{t',t}$ are worked out for SQWR's in our earlier work[10] in terms of the harmonic wave functions in the x direction and numerically in the z direction and will not be repeated here. In double wires, the electron-phonon matrix elements are calculated numerically for the ground state in the x direction and the tunnel-coupled ground doublets in the z direction between the initial (k) and the final ($k'=k\pm q_y$) states for one-phonon absorption ($+$) and emission ($-$) processes.[10] The phonons are assumed to be in equilibrium.

A. Single quantum wire

Figure 2 displays the conductance $G(B)$ of sample 1 as functions of $B||z$ by including only roughness scattering in panel (a) and only phonon scattering in panel (b). For this sample with large $\hbar\omega_x=2.5$ meV, only two lowest sublevels are populated (see the left insets). In Fig. 2(a), the position of the rough interface of sample 1 is shown by double vertical lines in the right inset. The conductance $G(B)$ is shown for several temperatures $T=0.25$ K (dash-dot-dotted curve), 1 K (dash-dotted curve), 4 K (dashed curve), and 16 K (solid curve). The abrupt rise of the conductance above $B=2$ T is due to the depopulation of the level $n=1$.[6,8] The level depopulation arises from the increasing mass m^{**} with B. The rapid decrease of the conductance with increasing temperature above 2 T is due to 1) to the thermal repopulation of the bottom of the level $n=1$ and 2) horizontal scattering from $n=0$ to the bottom of the $n=1$ sublevel. Here, a large density of states and a small group velocity contribute to increased scattering without contributing to a significant current. The phonon-limited $G(B)$ is shown in Fig. 2(b) for T

TABLE II. DQWR's with the wire width 42 Å in the x direction, QW widths L_{z1}, L_{z2}, center-barrier width L_B, total one-dimensional electron density n_{1D}, symmetric-antisymmetric (SAS) ground-doublet tunnel splitting Δ_{SAS} (at $B=0$), the wire length L_y, and the chemical potential μ (at $T=0$ K and $B=0$) relative to the bottom of the ground level.

Sample no.	L_{z1}/L_{z2} (Å)	L_B (Å)	n_{1D} (10^5 cm^{-1})	Δ_{SAS} (meV)	L_y (μm)	μ (meV)
3	80/80	40	6.5	3.6	1	3.79
4	80/80	50	6.5	1.6	1	2.57

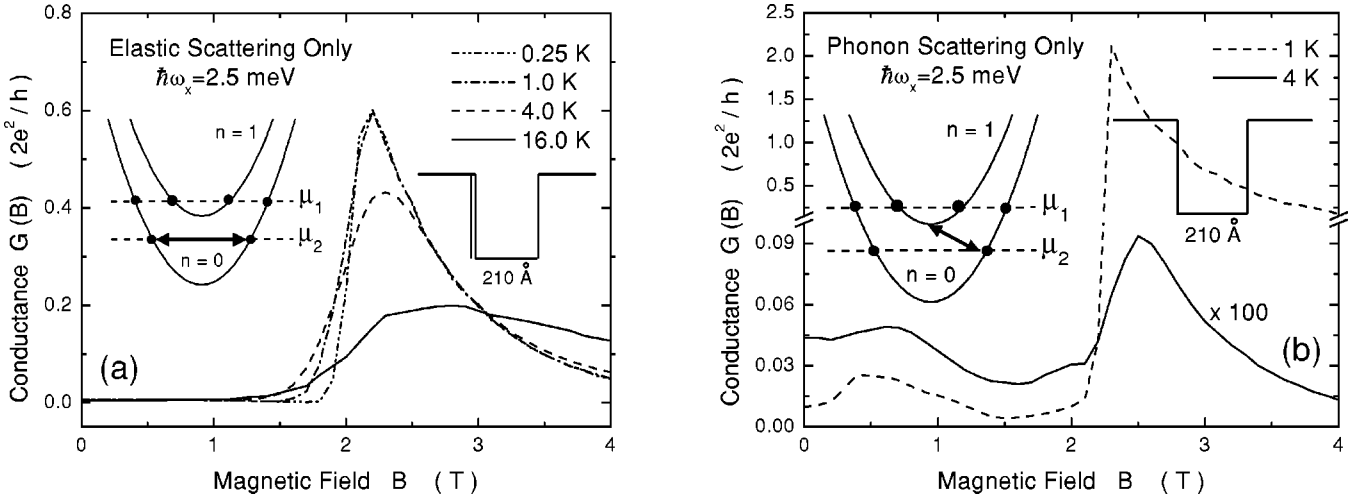

FIG. 2. Conductance $G(B)$ vs B for SQWR sample 1 including only roughness scattering in (a) and phonon scattering in (b) for several temperatures. The left insets in (a) and (b) display the energy dispersion for the two lowest sublevels $n=0$ and $n=1$. The dashed horizontal lines show the position of the chemical potential $\mu=\mu_1$ in the upper sublevel (for $B\leqslant 2$ T) and $\mu=\mu_2$ in the lower sublevel $n=0$ (for $B>2$ T). The thick double-headed arrows illustrate roughness scattering in (a) and phonon scattering in (b). The right insets illustrate the sample structure. The double vertical bars in the inset of (a) indicate the rough interface.

$=1$ K (dashed curve) and 4 K (solid curve). We see here that the conductance increases abruptly above $B=2.2$ T at $T=1$ K due to the level depopulation. Note that the conductance is to be replaced by the quantized conductance here and later, when it exceeds the ballistic value [i.e., $2e^2/h$ in Fig. 2(b)]. The sharp increase at $B=2.2$ T and 1 K in (b) is suppressed by phonon scattering by more than three orders of magnitude at 4 K (solid curve). This sensitive temperature dependence is caused by the requirement that a threshold phonon (illustrated by the double-headed arrow in the left inset) with a large momentum (and thus a large energy) is necessary for intersublevel scattering to yield efficient momentum dissipation. The initial increase of $G(B)$ at $B\leqslant 0.5$ T is attributed to the fact that backscattering between the Fermi points k and $-k$ is reduced because the wave functions at these states are pushed to the opposite directions by the Lorentz force under B. This initial increase is followed by a decrease of $G(B)$ between $0.7<B\leqslant 1.5$ T as the chemical potential is driven by B toward the low-conductance region near the bottom of the level $n=1$, where scattering is high due to the large density of states.

The conductance of sample 1 is displayed in Fig. 3 as a function of B for several temperatures when both the roughness and phonon scattering are included. Comparing Fig. 3 with Fig. 2(a), we see that roughness scattering is more significant than phonon scattering at $T=1$ K. However, phonon scattering dominates over roughness scattering in the range of $T\geqslant 2$ K. Phonon scattering suppresses $G(B)$ by more than an order of magnitude at temperatures as low as $T=2$ K (dash-dotted curve) and up to two orders of magnitude at $T=4$ K (solid curve). In fact, the resistance $\propto G^{-1}$ rises nearly as $\propto\exp(-\varepsilon_a/k_BT)$ above $T=1.7$ K at $B=2.5$ T with the activation energy $\varepsilon_a\sim 1.1$ meV close to the half of the sublevel gap $\hbar\omega_x=2.5$ meV of sample 1 (see Table I). The chemical potential is about halfway between the levels $n=0$ and $n=1$ at this field between $T=1$ and 2 K. The conductance saturates to the roughness-limited value at low temperatures $\ll 1$ K.

Figure 4 displays the conductance of sample 2 at $T=2$ K (dashed curve) and 4 K (solid curve), including both the roughness and the phonon scattering. For this sample, the sublevel spacing $\hbar\omega_x=1.6$ meV is smaller compared to sample 1, yielding three-level occupation (see the inset) at $B=0$ for the same electron density. This leads to two magnetoquantum oscillations of $G(B)$. Here, the conductance is

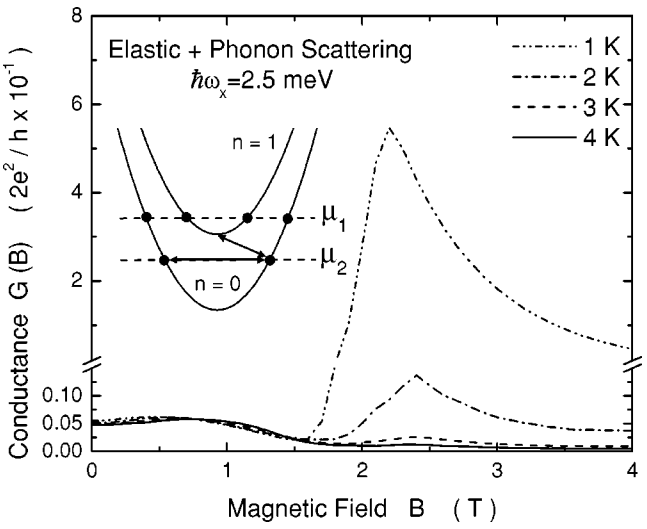

FIG. 3. Conductance $G(B)$ vs B for sample 1 including roughness and phonon scattering for temperatures $T=1$, 2, 3, and 4 K. The inset shows the energy dispersion for the two lowest sublevels $n=0$ and $n=1$. The dashed horizontal lines in the inset show the position of the chemical potential $\mu=\mu_1$ in the upper sublevel $n=1$ and $\mu=\mu_2$ in the lower sublevel $n=0$. The thick horizontal (tilted) double-headed arrow illustrates intrasublevel (intersublevel) roughness (phonon) scattering.

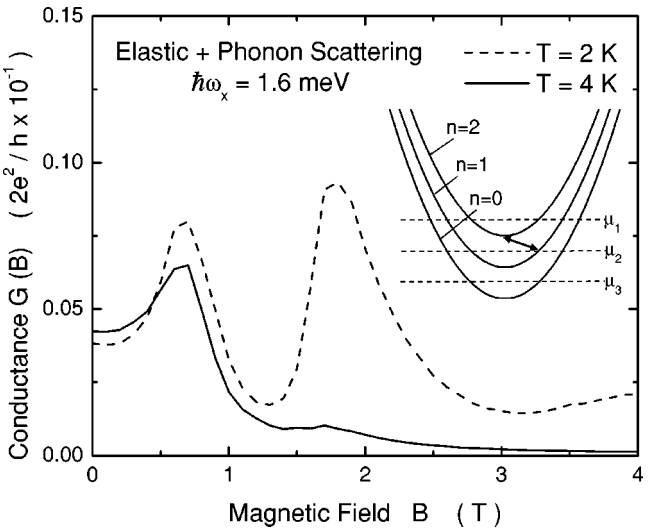

FIG. 4. Conductance $G(B)$ vs B for sample 2 including roughness and phonon scattering at $T=2$ and 4 K. The inset presents the energy dispersion for the three lowest sublevels with $n=0,1$, and 2. The dashed horizontal lines shows the position of the chemical potential μ above each sublevel $\mu=\mu_1$ for $B\leqslant 0.5$ T, $\mu=\mu_2$ for $0.5<B\leqslant 1.5$ T, and $\mu=\mu_3$ for $B>1.5$ T. The thick tilted double-headed arrow illustrates intersublevel phonon scattering.

smaller than in Fig. 3 at a given temperature and B due to enhanced phonon scattering involving smaller phonon energies and smaller $\hbar\omega_x$. The fact that the second conductance peak at $B=1.8$ T (dashed curve) is higher than the first peak around 0.7 T at 2 K is attributed to the same reason. Namely, the sublevel spacing $\hbar\Omega_x$ is much larger at 1.8 T requiring larger phonon energies for scattering and yielding reduced phonon scattering. When T is increased from 2 K to 4 K, the magneto-quantum oscillation of $G(B)$ around $B=2$ T is completely suppressed at $T=4$ K due to enhanced phonon scattering.

B. Double quantum wires

Figure 5(a) presents the conductance $G(B)$ of DQWR sample 3 as a function of B for several temperatures ranging from 1 K to 16 K by including only roughness scattering. The positions of the two rough interfaces are shown in its right inset. At low temperatures $T\leqslant 2$ K, the conductance is enhanced between $3<B<7$ T where the chemical potential is inside the gap as shown by $\mu=\mu_2$ in the left inset. This conductance enhancement arises from suppressed backscattering illustrated by the thick double-headed arrow in the inset between the initial and final scattering states at the Fermi points denoted by the two black dots. The suppression is due to a small overlap between the initial- and final-state wave functions which are separated into different QW's by the field. The dramatic rise of the conductance above $B\sim 7.5$ T at $T=16$ K arises from the following physics. The chemical potential is near the lower gap edge (e.g., at $\mu=\mu_3$ in the left inset) at this high field (away from the midgap area where the above discussed backscattering is weak), yielding a small conductance at low temperatures as shown by the dash-dotted and dash-double-dotted curves for $1\leqslant T\leqslant 2$ K in Fig 5(a). At high temperatures (e.g., $T=16$ K), however, the electrons are activated to populate the weak-scattering highly conducting midgap states near μ_2, yielding giant conductance peak as shown. A similar but less pronounced effect is also seen from the dotted curve at $T=8$ K.

Figure 5(b) shows the conductance for the same sample (sample 3) when only phonon scattering is present at T

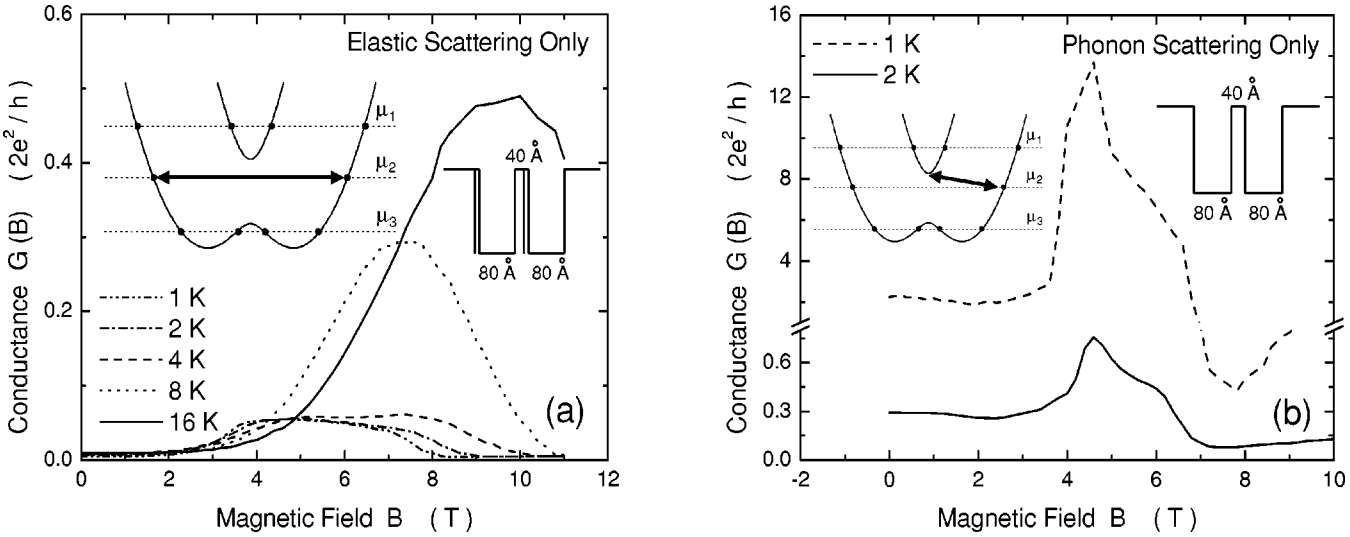

FIG. 5. Conductance $G(B)$ vs B for several temperatures for DQWR sample 3 including only roughness scattering in (a) and phonon scattering in (b). The left insets display the energy dispersion of the two tunnel-split branches. The dashed horizontal lines show the position of the chemical potential $\mu=\mu_1$ above the gap (for $B\leqslant 3$ T), $\mu=\mu_2$ inside the gap (for $3<B\leqslant 7$ T), and $\mu=\mu_3$ below the gap (for $B>7$ T). The thick horizontal (tilted) double-headed arrow in the insets illustrates the roughness-(phonon-) scattering processes within (across) the tunneling gap, respectively. The right inset in (a) illustrates the sample structure including the position of the two rough interfaces indicated by double vertical bars.

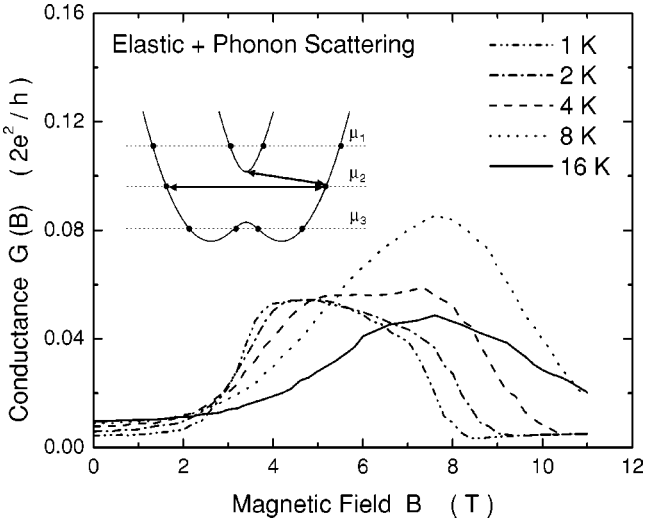

FIG. 6. Conductance $G(B)$ vs B for several temperatures for DQWR sample 3 including both roughness and phonon scattering. The inset displays the energy dispersion of two tunnel-split branches. The dashed horizontal lines in the inset show the position of the chemical potential $\mu=\mu_1$ above the gap, $\mu=\mu_2$ inside the gap, and $\mu=\mu_3$ below the gap. The thick horizontal (tilted) double-headed arrow illustrates roughness (phonon) scattering.

$=1$ K (dashed curve) and 2 K (solid curve). Phonon scattering is severely suppressed at $T=1$ K, yielding a peak for $G(B)$ when the chemical potential lies at $\mu=\mu_2$ inside the tunneling gap as shown in the left inset for $3<B<7$. At $T=2$ K, however, phonons can efficiently scatter the electrons from the Fermi points at $\mu=\mu_2$ to the bottom of the upper branch as shown by the thick double-headed arrow in the left inset. The initial and final wave functions have a large overlap for this scattering process because the wave functions near the bottom of the upper branch have amplitudes on both wires, reducing $G(B)$ by an order of magnitude from the conductance at $T=1$ K inside the gap as shown by the solid curve.

Figure 6 shows the conductance of the same sample (sample 3) in the presence of roughness and phonon scattering at several temperatures. By comparing the figure with Fig. 5(a), it is clear that roughness scattering dominates over phonon scattering for $T\leqslant 4$ K. At high temperatures $T\geqslant 8$ K, however, the large conductance enhancement shown by the dotted and solid curves above $B=7$ T in Fig. 5(a) is suppressed by the phonon-scattering effect, making the conductance peak smaller for $T=16$ K than for 8 K in Fig. 6 in contrast to Fig. 5(a).

In Fig. 7, we compare the conductance enhancements $G(B)/G(0)$ of samples 3 and 4 at $T=2$ K with both roughness and phonon scattering in panel (a) and with only roughness scattering in panel (b). Sample 4 is the same as sample 3 except that the center-barrier thickness L_B is larger, resulting in a much smaller tunneling gap. As a result, phonon scattering across the gap requires a smaller activation energy and becomes more efficient in sample 4, making the conductance enhancement factor of sample 4 (dashed curve) smaller than that of sample 3 (solid curve) as shown in Fig. 7(a). In contrast, the conductance enhancement of sample 4 (dashed curve) is much larger than that of sample 3 (solid curve) inside the gap in the absence of phonon scattering as shown in Fig. 7(b) because of a smaller overlap between the two Fermi points for backscattering for sample 4. By comparing Fig. 7(a) and Fig. 7(b), we note that the enhancement for sample 3 (with $L_B=40$ Å, solid curves) is hardly affected by phonon scattering at 2 K, while it is suppressed for sample 4 (with $L_B=50$ Å, dashed curves) by nearly an order of magnitude in Fig. 7(a).

In order to elucidate further the role played by phonon scattering, we present in Fig. 8 the temperature dependence of the conductance of sample 3 for several fields. The con-

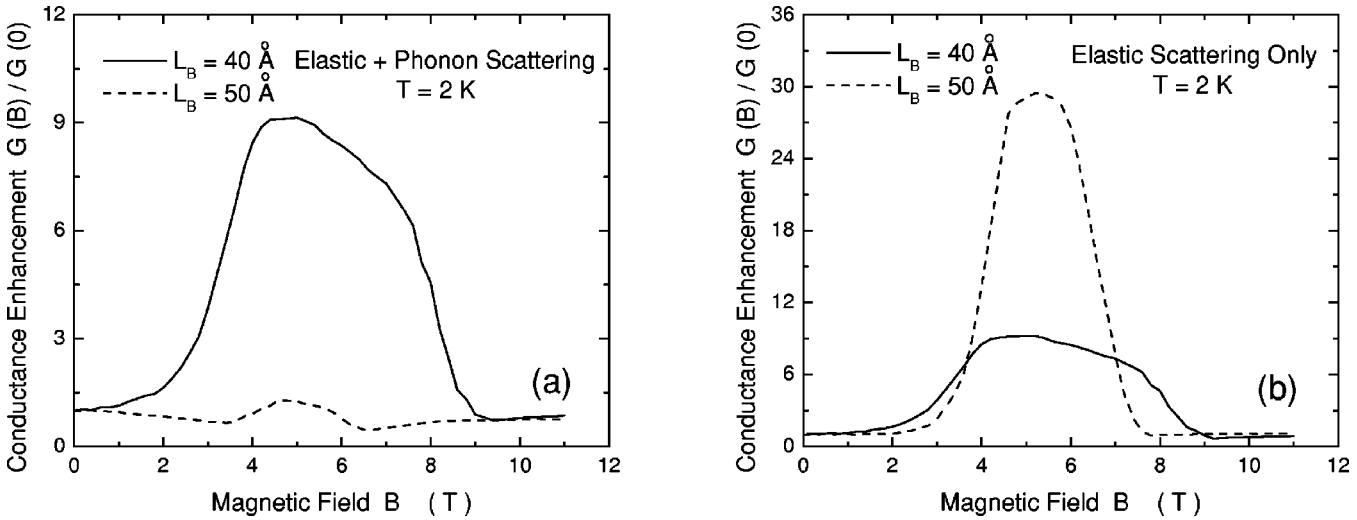

FIG. 7. Comparisons of $G(B)/G(0)$ vs B for samples 3 and 4 with different center-barrier thickness $L_B=40$ Å (solid curves) and $L_B=50$ Å (dashed curves) at $T=2$ K including both roughness and phonon scattering in (a) and only roughness scattering in (b). Other parameters are the same for these two samples

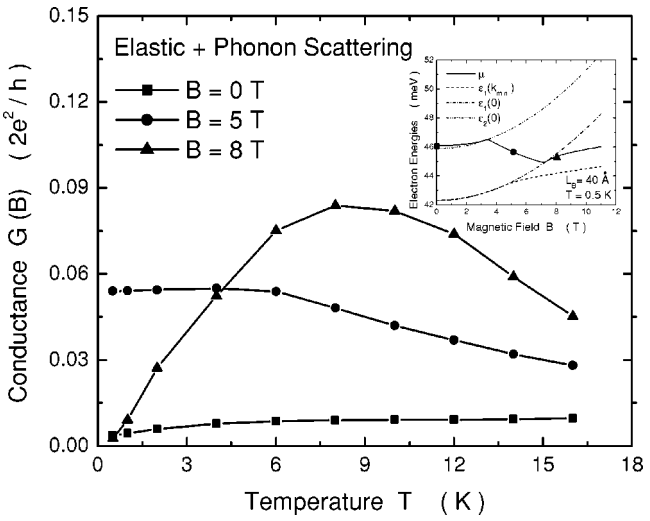

FIG. 8. Conductance $G(B)$ vs T for several fields for DQWR sample 3 including roughness and phonon scattering. The inset of the figure shows the positions of the chemical potential (solid curve), the bottom of the upper branch (dash-double-dotted curve), the lower gap edge (dash-dotted curve), and the bottom of the lower branch (dashed curve).

ductance at $B=5$ T is relatively large at $T=1$ K because the chemical potential is near the midgap as seen from the inset by the solid circle. As the temperature increases, the conductance drops at this field because the electrons can be scattered and thermally activated to the bottom of the upper branch, where the conductance is much smaller as discussed earlier. The inset shows the position of the chemical potential relative to the gap edges shown by dash-dotted and dash-double-dotted curves. The dashed curve indicates the bottom of the lower branch. At $B=8$ T, the chemical potential is just below the gap as shown by the solid triangle in the inset. The electrons are activated to the highly conducting midgap region with increasing temperature, explaining the rapid rise of the conductance with the temperature. However, the conductance drops after a peak above $T=8$ K due to phonon scattering.

V. CONCLUSIONS

We presented a rigorous numerical formalism for calculating the conductance to a desired accuracy in quasi-one-dimensional systems in the presence of elastic and phonon scattering. The formalism was employed to study the effects of phonon scattering and interface-roughness scattering at low temperatures on the temperature-dependent electron conductance in a multilevel single [see Fig. 1(a)] and tunnel-coupled double [see Fig. 1(b)] quantum wires under a perpendicular magnetic field. Deformation-potential and piezoelectric interactions were assumed for phonon scattering at low temperatures, while monolayer fluctuation was considered for interface-roughness scattering. The effect of phonon scattering is found to be significant when the thermal energy is comparable to the energy separation between the Fermi level and the nearest unoccupied sublevel in SQWR's and to the tunneling gap energy in DQWR's.

For SQWR's, the large conductance enhancement [see Fig. 2(a)] obtained when the chemical potential falls below the bottom of a sublevel in the presence of elastic scattering alone was shown to be suppressed by phonon scattering even at low temperatures (see Fig. 3). While the magnetoconductance is expected to decrease with rising temperature in general, it displays a strikingly opposite behavior in certain field and temperature regimes in DQWR's. This interesting situation occurs when the chemical potential lies near or just below the lower edge of the anticrossing gap as shown by μ_3 in the insets of Figs. 5(a) and 5(b). In this case, the electrons are activated to the middle of the gap shown by μ_2 in the insets where the conductance is very high. This behavior is shown by the rapid rise of the conductance in Fig. 8 at $B=8$ T as a function of the temperature. After reaching a maximum around $T=8$ K, however, the conductance decreases rapidly with T due to phonon scattering as shown by the curve for 8 T.

ACKNOWLEDGMENTS

The authors thank Dr. M. P. Lilly for helpful comments on the manuscript. Sandia is a multiprogram laboratory operated by Sandia Corporation, a Lockheed Martin Company, for the U.S. DOE under Contract No. DE-AC04-94AL85000.

[1] J. Lee and H.N. Specor, J. Appl. Phys. **54**, 3921 (1983).
[2] G. Fishman, Phys. Rev. B **34**, 2394 (1986).
[3] H. Sasaki, T. Noda, K. Hirakawa, M. Tanaka, and T. Matsusue, Appl. Phys. Lett. **51**, 1934 (1987).
[4] S. Das Sarma and X.C. Xie, Phys. Rev. B **35**, 9875 (1987).
[5] K.F. Berggren, G. Roos, and H. van Houten, Phys. Rev. B **37**, 10 118 (1988).
[6] H. Akira and T. Ando, Phys. Rev. B **43**, 11 676 (1991).
[7] B. Tanatar and A. Gold, Phys. Rev. B **52**, 1996 (1995).
[8] S.K. Lyo and D. Huang, Phys. Rev. B **64**, 115320 (2001).
[9] T. Sugaya, J.P. Bird, M. Ogura, Y. Sugiyama, D.K. Ferry, and K.Y. Yang, Appl. Phys. Lett. **80**, 434 (2002).
[10] S.K. Lyo and D. Huang, Phys. Rev. B **66**, 155307 (2002).
[11] J.M. Ziman, *Principles of the Theory of Solids*, 2nd ed. (Cambridge University Press, Cambridge, 1972), p. 215; W. Kohn and J.M. Lüttinger, Phys. Rev. **108**, 590 (1957).
[12] T. Holstein, Ann. Phys. (N.Y.) **29**, 410 (1964).
[13] S.K. Lyo, Phys. Rev. B **50**, 4965 (1994).
[14] S.V. Korepov and M.A. Liberman, Phys. Rev. B **60**, 13 770 (1999).